Scientia Iranica B (2021) 28(5), 2639–2654

Sharif University of Technology
**Scientia Iranica**
*Transactions B: Mechanical Engineering*
http://scientiairanica.sharif.edu

# Study on parameter's optimization for the minimizing of the residual stress in powder mixed near-dry electric discharge machining

**S. Sundriyal[a], Vipin[a], and R.S. Walia[b,*]**

a. *Department of Mechanical Engineering, Delhi Technological University, Delhi, 110089, India.*
b. *Department of Production and Industrial Engineering, Punjab Engineering College, Chandigarh, 160012, India.*

Received 8 May 2020; received in revised form 7 November 2020; accepted 30 August 2021

**KEYWORDS**
Residual stress;
EDM;
Powder;
Near dry;
X-ray method.

**Abstract.** The products processed by Electrical Discharge Machining (EDM) leave some undesirable effects, the most prominent of which is Residual Stress (RS). These RS affect fatigue behavior, dimensional stability, and stress corrosion. The latter is the cause of failure of processed products. It has been observed that products obtained by Powder Mixing Near Dry Electric Discharge Machining (PMND-EDM) have relatively low RS values. The purpose of this research is to minimize the RS caused in the machined workpiece (EN-31) by optimizing the process parameters that significantly affect the machining characteristics. The selected parameters were tool diameter, mist flow rate, metal powder concentration, and mist pressure, and the selected workpiece was EN-31 because it has ideal mechanical properties and is widely used in manufacturing. The minimum value of RS at optimized values of process parameters was found to be 106.32 MPa.



## 1. Introduction

Electric Discharge Machining (EDM) was developed in 1943 by Russian scientist Lazarenko. EDM is one of the non-conventional machining methods which utilize thermal energy for material removal from the workpiece. Today, EDM is widely used in global manufacturing engineering. This technology makes it possible to cut complex shapes on very hard materials. Further study of EDM by the researchers has led to the development of various hybrid EDM machining methods such as Dry Electric Discharge Machining (D-EDM), Near Dry EDM (ND-EDM), Powder Mixed EDM (PM-EDM), and Powder Mixed Near Dry EDM (PMND-EDM). These developed methods were more prominent in terms of machining efficiency. ND-EDM uses gas mist and a small amount of dielectric oil as the dielectric, so unlike traditional EDM, this machining method also eliminates a large amount of EDM oil required [1]. The feasibility of the new EDM process which was known as PMND-EDM came into existence [2]. Gases such as nitrogen or air as a dielectric medium instead of dielectric oil were used in DEDM which makes processing eco-friendly as this new methodology produces less harmful fumes and at the same time also eliminates the need for EDM oil [3].

Previous research has been conducted on PM-EDM for performance enhancements such as improved Material Removal Rate (MRR), Tool Wear Rate (TWR), surface finish (Ra), and morphology. A study on machining efficiency was performed for PMEDM and Taguchi $L_9$ (OA) was utilized for optimization. The results show that PMND-EDM can reduce TWR and residual stress due to the stable arc conditions at the gap between the electrodes [4]. Rotary tool elec-

*. *Corresponding author. Tel.: +91 9717325233*
*E-mail address: waliaravinder@yahoo.com (R.S. Walia)*

doi: 10.24200/sci.2021.55837.4429

trode was used as in NDEDM and there was enhanced MRR with improved surface finish with reduced microcracks and debris accumulation [5]. Similarly, oxygen gas was utilized as a dielectric medium in NDEDM and it was reported that more MRR was observed with the increasing phenomenon of melting by rapid oxidation [6]. The experimental result and analysis showed that PMND-EDM was a better machining method than ND-EDM because in the former technique, the MRR is increased by 45.04%, while surface and TWR are reduced by 45.33% and 60.60%, respectively [7]. It was also noticed that PMND-EDM resulted in producing a machined surface with better surface quality due to the presence of metallic foreign particles in the dielectric medium which leads to a stable arc at the machining gap [8].

The study has also been performed in the field of surface morphology such as improved microhardness in PM-EDM. The presence of hard tungsten carbide ($W_2C$) and cementite ($Fe_3C$) increased the MH ($\sim$ 150%) on the machined surface [9]. The formation of carbides on the machined surface increased the microhardness to 912 HV without sacrificing the quality of the machined surface [10]. Taguchi's philosophy was adopted to determine the suitable combination of EDM parameters to improve machining performances in terms of material removal and micro-hardness [11].

Products made by different EDM methods have a variety of adverse effects on components, and the residual stress generated on the working surface is the main one. The metallurgical transformation caused by the sharp temperature gradient is the cause of the residual stress in the mechanical parts [12]. It is found that the strength of this residual stress is greater than the yield point of the material, which will cause serious cleavage, twinning, and slippage in the crystal structure [13]. The nature of residual stress was investigated and it was revealed that high residual stresses were found at the immediate surface of the machined sample and then gradually falls to a low value before giving a small way to compressive residual stresses [14]. Compared with the ND-EDM process, the residual stress of the PMND-EDM machined surface is reduced by 56.09% [15]. A hard layer of zinc carbide is deposited on the surface of the processed sample, which led to a higher microhardness value [16]. A peak value of residual stress in EDM was investigated on the machined surface of the workpiece and it was concluded that residual stress with a peak value of 590 MPa was found at 40 $\mu$m beneath the top surface of the workpiece and was reduced to zero value at 200 $\mu$m depth [17]. EDM results in the generation of residual stresses of high value which increase from the surface and reach the maximum value. This maximum value is around the ultimate tensile strength of the material [18]. Optimization of the residual stress using X-ray $\cos\alpha$ method in vibration-assisted hybrid EDM process was performed over high carbon high chromium D2 tool steel workpiece. The results show that discontinuous vibrations enhanced the MRR and reduced the residual stresses induced in the machined workpiece [19]. The finite element method was used to model the residual stress of the EDM workpiece. It was revealed by the study that the value of residual stresses at the subsurface of the workpiece was more than the top surface due to high surface roughness on the top surface and low discharge energy of the sparks was attributed to lower values of the residual stresses [20]. Finite element analysis of residual stresses in EDM was performed and techniques like nano-indentation technique and Raman spectroscopy were adopted to measure the residual stress in the AISI H13 tool steel machined by EDM process and it was revealed that microcracks which were responsible for relieving some part of residual stress [21]. A parametric study for residual stresses was performed in wire EDM and the Taguchi method of optimization was utilized to minimize the residual stresses in the aluminum workpiece [22].

There are many factors that are responsible for the residual stress such as heating, cooling, re-solidification, melting, and phase transformations with volume change. This induced residual stress results in a decrease in the reliability of the product and at the same time leads to uncertain failure of the manufactured products. Therefore, it is necessary to study residual stresses in order to minimize these stresses and improve product reliability. These residual stresses are generated in the specimens due to a heating phenomenon and re-solidification on the surface of the workpiece. Thus this residual stress plays a vital role in determining product quality and reliability. Although studies on performance enhancements and optimization techniques have been applied in PM-EDM still investigations related to residual stress and optimization of critical parameters in PMND-EDM are still lacking therefore in this study contributions and efforts have been made to explore the important mechanical property (RS) of the machined products. This research could help further in-depth studies in the field of residual stress optimization and could provide the ground for conducting research in the field of PMND-EDM [16].

## 2. Experimentation

### *2.1. Experimental procedure*

The experimental process parameters are divided into six categories: dielectric, metal powder, tools, electrical parameters, workpieces, and other parameters (air pressure, oil pressure, and mist flow rate). Series of experiments were performed according

**Table 1.** Residual stress experimental results according to Taguchi $L_9$ OA.

| Experiment no. | Parameteric conditions | | | | Residual Stress (RS) (MPa) | | | S/N (decibel) |
|---|---|---|---|---|---|---|---|---|
| | *A* | *B* | *C* | *D* | Run 1 | Run 2 | Run 3 | |
| 1 | 2 | 5 | 2 | 0.4 | 565 | 558 | 530 | –54.82 |
| 2 | 2 | 10 | 5 | 0.5 | 621 | 551 | 550 | –55.19 |
| 3 | 2 | 15 | 8 | 0.6 | 510 | 659 | 678 | –55.85 |
| 4 | 3 | 5 | 5 | 0.6 | 370 | 361 | 340 | –51.05 |
| 5 | 3 | 10 | 8 | 0.4 | 145 | 169 | 186 | –44.48 |
| 6 | 3 | 15 | 2 | 0.5 | 239 | 279 | 280 | –48.51 |
| 7 | 4 | 5 | 8 | 0.5 | 251 | 214 | 311 | -48.35 |
| 8 | 4 | 10 | 2 | 0.6 | 230 | 209 | 191 | –46.46 |
| 9 | 4 | 15 | 5 | 0.4 | 556 | 501 | 587 | –54.79 |
| Total | – | – | – | – | 3478 | 3501 | 3653 | – |
| Mean | – | – | – | – | 386.44 | 389 | 405.88 | – |
| Overall mean RS ($\overline{RS}$) = 394.11 MPa | | | | | | | | |

to Taguchi $L_9$ (OA) for residual stress. Each series of experiments was carried out 3 times, and the results are shown in Table 1.

The experimentation methodology was derived from previous work in the field of EDM [15,16]. Each series of experiments were carried out in three runs. By considering the better principle given by $S/N$ (Signal-to-Noise ratio) in Eq. (1), a total of 27 experiments were carried out to analyze residual stress [16]:

$$S/N = -\log_{10}\left(\frac{1}{n}\sum_{i=1}^{n} y_{ij}^2\right), \quad (1)$$

where $n$ is replications, and $y_{ij}$ is response value.

The standard deviation error bar between the mean value of the obtained residual stress for different parametric experimental conditions was plotted (total twenty-seven experiments: three repeatabilities for each set of parametric conditions) and the error was within $+/-5\%$ range as shown in Figure 1.

Residual stress measurement techniques can be divided into different categories, such as destructive testing, semi-destructive testing, and Non-Destructive Testing (NDT). NDT has several advantages over semi-destructive and destructive testing. NDT can be applied to a wide variety of materials and the accuracy of measurement is high. There are many NDT methods for measuring residual stress, such as X-ray diffraction technology, Burkhausen noise method, neutron diffraction method, and ultrasonic method. The X-ray diffraction method has several advantages over other methods because the X-ray diffraction technique can be used to measure the residual stress of a variety of materials. Another advantage of X-ray diffraction technology is that it can analyze microscopic and macroscopic residual stresses. At the same time, the technology is handheld and can be read in any direction.

The residual stress measurement is performed by a $\mu$X-360 pulsetec machine (made in Japan), as shown in Figure 2. It is mainly composed of three parts: computer, sensor unit, and power supply unit. The setup consists of the X-ray tube (30 KV) and 2-D X-ray sensor for visual analysis along with a power supply unit to generate the X-ray.

The X-ray takes 90 seconds to take one reading of residual stress. The machine has a special func-

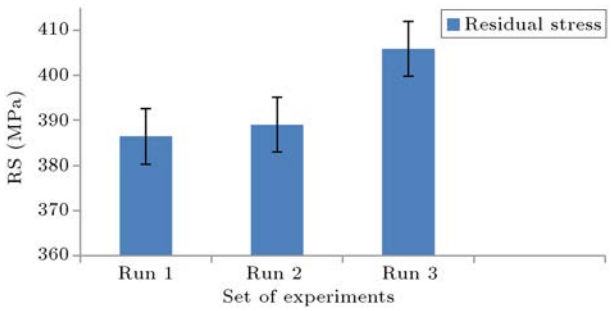


**Figure 1.** Standard deviation error bar for residual stress for different set of experiments.

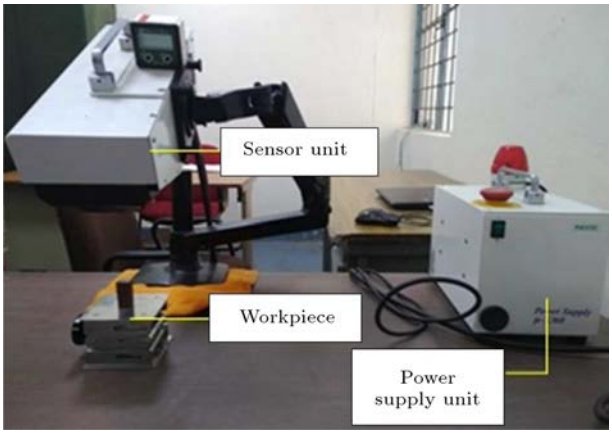


**Figure 2.** Portable XRD - residual stress analyzer in operation.

tion of air cooling, which can achieve high-efficiency performance. The X-ray tube current was 1 mA and the sample distance from the X-ray focusing lens was 38 mm. The incident angle for the X-ray was adjusted at 35 degrees while the information regarding the specimen to be analyzed were lattice constant, interplanar spacing and diffraction planes ($h$, $k$, $l$), and crystal structure, Poisson's ratio, and Young's modulus. The measured output responses were residual stress, shear stress, and full width half maximum value. The Full Width Half Maximum (FWHM) is the expression of the function range (profile peak diffraction), and the maximum and minimum peak diffraction are expressed as $\alpha$-max and $\alpha$-min, respectively. The procedure of residual stress measurement is divided into four stages. The first stage includes sample positioning and capture of the sample image. The second stage includes the incidence of the X-ray and its detection by a 2-D sensor. The third stage includes the calculation of residual stress and the final stage includes output data results of residual stress and value of FWHM. The output reading also calculates the standard deviation of the obtained readings to maintain the repeatability of reading. The working principle of residual stress is based on X-ray diffraction scattering and it is in agreement with Bragg law given by Eq. (2) [23]:

$$n\lambda = 2d \sin\theta, \tag{2}$$

where $n$ is the order of reflection; $d$ is the interplanar spacing of the crystal; $\lambda$ is the wavelength of the incident X-ray; and $\theta$ is the angle of incidence that equals the angle of scattering (diffraction angle) as shown in Figure 3. X-ray diffraction occurs from various orientations of the grain crystals that satisfy Bragg's law as shown in Figure 4. The diffracted X-ray form a cone around the incident X-ray axis because of the variation in crystal's orientation which also results in the formation of a ring of residual stress known as the Debye-Scherrer ring as shown in Figure 5. This Debye ring is formed by the single short-duration X-ray exposure. Determination of the residual stress is

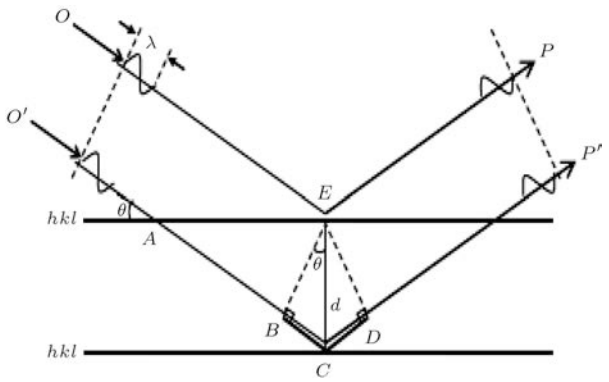


**Figure 3.** Diffraction orientation of incident X-ray from the sample.

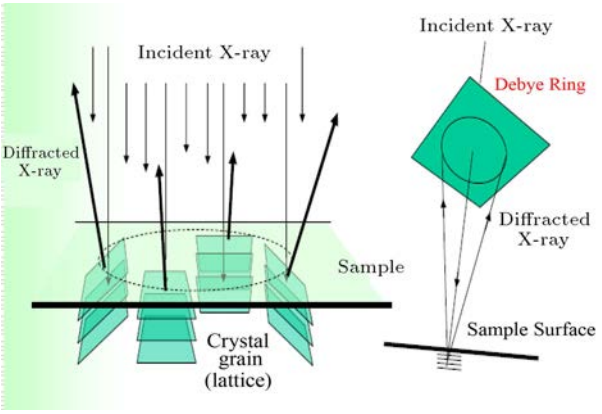


**Figure 4.** Formation of Debye-Scherrer ring.

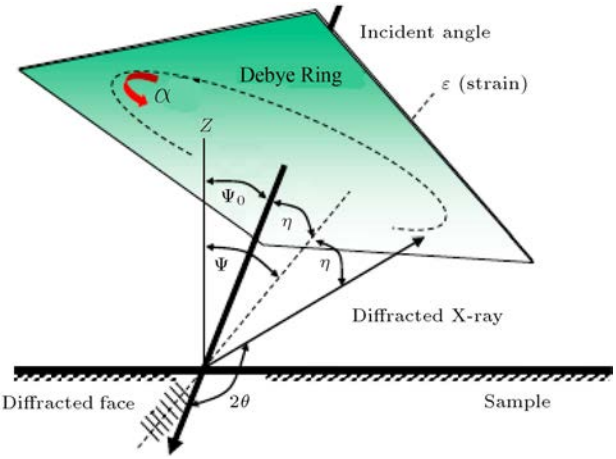


**Figure 5.** Scattering phenomenon of diffracted X-ray.

achieved by accurately measuring the position of the Debye- Scherrer rings and their positions are a direct measure of strain.

The magnitude of the strain is determined by the position of the detected Debye-Scherrer ring and is calculated by using the formula given in Eqs. (3) and (4). The residual stress and shear stress are calculated by Eqs. (5) and (6):

$$\varepsilon_{\alpha 1} = \frac{1}{2}\left\{(\varepsilon_{\alpha} - \varepsilon_{\pi+\alpha}) + (\varepsilon_{-\alpha} - \varepsilon_{\pi-\alpha})\right\}, \tag{3}$$

$$\varepsilon_{\alpha 2} = \frac{1}{2}\left\{(\varepsilon_{\alpha} - \varepsilon_{\pi+\alpha}) + (\varepsilon_{-\alpha} - \varepsilon_{\pi-\alpha})\right\}, \tag{4}$$

$$\sigma_x = -\frac{E}{1+\vartheta} * \frac{1}{\sin 2\eta} * \frac{1}{\sin 2\varphi^o} * \frac{\partial \varepsilon\alpha 1}{\partial \cos\alpha}, \tag{5}$$

$$T_{xy} = -\frac{E}{2(1+\vartheta)} * \frac{1}{\sin 2\eta} * \frac{1}{\sin 2\varphi^o} * \frac{\partial \varepsilon\alpha 2}{\partial \sin\alpha}, \tag{6}$$

where $\alpha$ is the Azimuth angle of Debye-Sherrer ring; $\varepsilon\alpha_1$ is the strain measured in the vertical direction; $\varepsilon_{\pi+\alpha}$ is the strain measured in the direction of $\pi + \alpha$; $\sigma_x$ is the residual stress; $\tau_{xy}$ is the residual shear

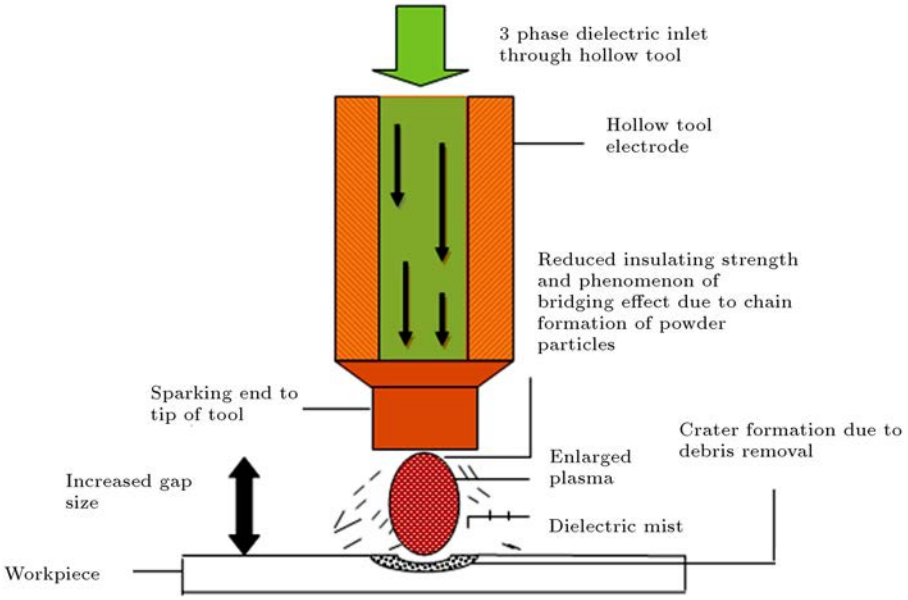


**Figure 6.** Schematic diagram of the working principle of Powder Mixing Near Dry Electric Discharge Machining (PMND-EDM).

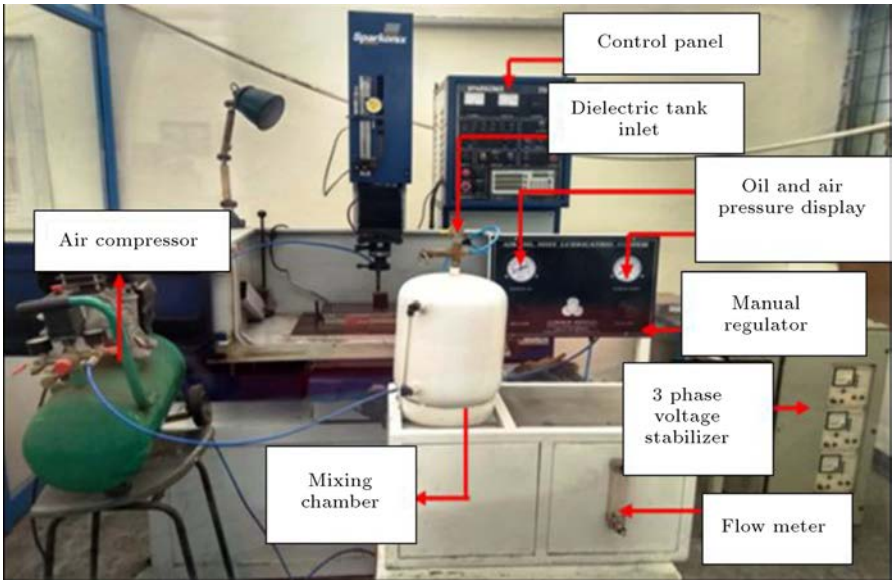


**Figure 7.** Indigenously developed setup for Powder Mixing Near Dry Electric Discharge Machining (PMND-EDM).

stress; $\nu$ is Poisson's ratio; $\varepsilon\alpha_2$ is the strain measured in the horizontal direction; $E$ is Young's modulus; $\eta$ is the angle between Debye-Scherrer ring axis and the sample diffraction detector X-ray; and $\varepsilon$ is the Poisson's ratio.

## 3. Method and developed setup

The schematic diagram for the working principle of PMND-EDM is shown in Figure 6. A newly designed setup of PMND-EDM was made indigenously at the precision engineering lab (DTU, Delhi) as shown in Figure 7 [4]. The setup developed for PMND-EDM includes various technical features and components designed and manufactured according to the required experimental conditions to achieve the desired output results. The setup body is made of stainless steel and consists of an EDM oil pressure regulator, an air pressure regulator, and a mist flow controller.

The pressure gauges were analogous in nature with a limit up to 0.6 MPa. The mist flow regulator was mounted on the setup together with a transparent scale, and the scale was up to 20 ml $min^{-1}$. It is as per the our setup developed and its specification. A separate air compressor (built-in Nu-Air) with a power of 2 H.P (horsepower), a pressure limit of 0.8

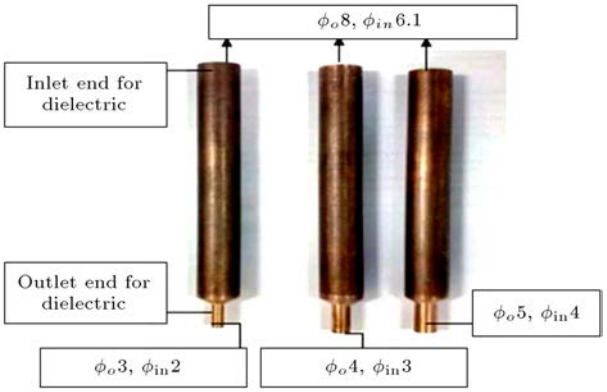


**Figure 8.** Developed copper tool electrodes for experiments (all dimensions are in mm).

MPa, and a capacity of 24 liters was integrated with setup. The mixing chamber was equipped with a setup for obtaining a 3-$\phi$ (phase) mixture of metal powder, glycerin (a stabilizer), and EDM oil, and compressed air supplied separately from an air compressor (Glycerin 5% dielectric oil, metal powder 2% dielectric oil). With the help of a flexible plastic tubes, the generated dielectric mist was provided at the EDM machining gap between the tool electrode and the workpiece. The experiments were performed on the Sparkonix EDM machine (Sparkonix limited Pune, 35 A series). Customized copper tool electrodes of different dimensions with special design features were fabricated and developed at the precision engineering lab (DTU, Delhi) as shown in Figure 8. The concept of the design of tool electrodes was taken from a previous study in the field of NDEDM [24]. The detailed design features of the hollow tool electrode are shown in Figure 9. A flexible tube of 6 mm is inserted into the inlet end of the tool for conveying the pressurized mist of the dielectric medium. The electrode sizes of different tools used in the experiment are shown in Table 2. The experimental conditions set for PMND-EDM are shown in Table 3, while the chemical and physical properties of the tool electrode are shown in Table 4.

The workpiece chosen for machining was EN-31 grade due to its desirable physical properties such as high strength and hardness. The chemical composition and physical properties of the EN-31 workpiece are shown in Table 5.

**Table 2.** Tool dimensions for experiments.

| Tool 1 | Tool 2 | Tool 3 |
|---|---|---|
| $d_i = 2; d_o = 3$ | $d_i = 3; d_o = 4$ | $d_i = 4; d_o = 5$ |

$d_i$= inner dia; $d_o$ = outer dia; All dimensions are in mm.

## 4. Working principle of PMND-EDM

The working principle of EDM is to convert electrical energy into heat energy. When current was supplied to the electrode, a plasma channel with high heat energy is generated at the working gap between the tool and the workpiece or the electrode gap. The ionization effect takes place due to the interaction of ions and molecules at this gap which results in generating a spark that jumps from tool to workpiece in case of straight polarity and vice versa. This repetitive cycle generates thousands of sparks which results in the formation of a plasma of very high temperature. This plasma channel of high heat energy is responsible for melting and removing material from the workpiece following which the erosion process starts. With the help of the dielectric oil supplied at the working gap, the erosion of the debris was flushed. The dielectric in PMND-EDM is composed of metal powder, compressed air, a very small amount of EDM oil, and glycerin used as a stabilizer. The metal powder acts as an additive, helping to form a chain structure of powder particles in the plasma channel, thereby reducing the dielectric strength of the dielectric medium and contributing to rapid corrosion. The compressed air supplied by the compressor helps to form the dielectric mist, and also helps to stabilize the arc at the gap between the electrodes due to the increase in the pressure of the supplied mist. The glycerol liquid which has high

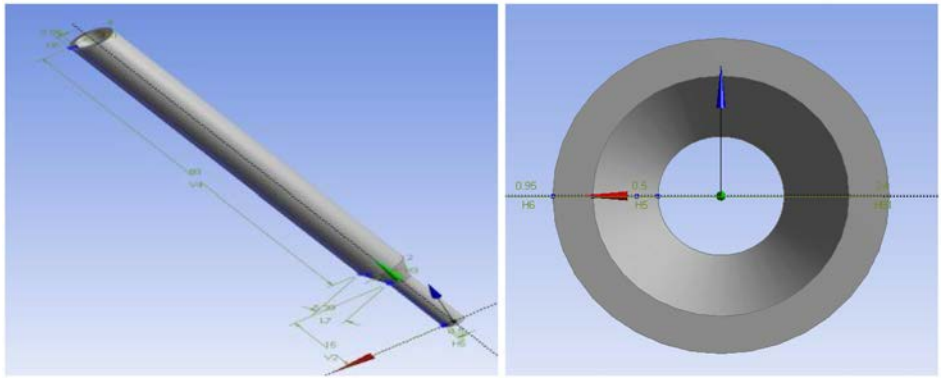

**Figure 9.** Design feature of the developed tool.

**Table 3.** Condition for experimental machining.

| Parameter | Description |
|---|---|
| Workpiece/tool | EN-31 (30 mm ×15 mm ×15 mm)/copper |
| Dielectric medium | Metallic powder + Air + oil (LL-221) + stabilizing agent |
| Current | 12 A |
| Gap voltage | 25 V |
| Pulse on/off | 500 $\mu$s/ 75 $\mu$s |
| Polarity | +ve |
| Tool diameter (mm) | 2, 3, 4 |
| Concentration of metallic powder | 2, 5, 8 (g $l^{-1}$) |
| Flow rate of dielectric medium | 5, 10, 15 (ml $min^{-1}$) |
| Pressure of dielectric | 0.4, 0.5, 0.6 (MPa) |
| Metallic powder | Zinc |
| Grain size of powder | 15 $\mu$m |
| Stabilizing agent | Glycerol (5%) |
| Machining time | 10 mins |

**Table 4.** Chemical and physical properties of tool.

| Properties | Values |
|---|---|
| Bulk modulus (Gpa) | 140 |
| Tensile strength (MPa) | 33.3 |
| Hardness (Mohs) | 2.5–3 |
| Thermal conductivity ($Wm^{-1}$ $K^{-1}$) | 385 |
| Boiling point (°C) | 2567 |
| Melting point (°C) | 1083 |
| Density (kg $m^{-3}$) | 8960 |
| Atomic number | 29 |
| Atomic weight | 63.546 |

viscosity was added to prevent the powder particles from settling down. This mixture is fed into the mixing chamber from the inlet of the tank and this heterogeneous mist is supplied at IEG (Inter Electrode Gap or gap between the tool and the workpiece) 25 $\mu$m at high pressure with the help of tubes from the mixing chamber. The current is supplied to the electrodes as soon as the experimental conditions are obtained. The sparking phenomenon starts and the erosion cycle takes place. The increased working gap due to the presence of metal powder results in a more uniform energized plasma. The reason for the increase in working gap and excited plasma is that the interlocking of powder particles at the IEG leads to the formation of chains of powder particles, which leads to high-frequency rapid sparks. The schematic diagram of setup is given in Figure 10.

The three-phase dielectric is supplied by hollow copper electrode tools in the final stage of the machining area. The compressed air is supplied to the mixing chamber. The compressed air is mixed with dielectric EDM oil and metal powder additives. Then, through the pressure control regulator, the dielectric mixture is supplied to the hollow tool electrode through the plastic tube. The dielectric is ejected from the other end of the electrode and starts to spark when power is supplied to the tool electrode. This method of injecting heterogeneous mist into the gap between the

**Table 5.** Chemical composition and physical properties of the workpiece (EN-31).

| Chemical properties | | Physical properties | |
|---|---|---|---|
| Element | % | Thermal conductivity (W $m^{-1}K^{-1}$) | 44.5 |
| Carbon | 0.90–1.20 | Hardness (HRC) | 63 |
| Silicon | 0.10–0.35 | Yield stress (MPa) | 450 |
| Manganese | 0.30–0.75 | Melting point (°C) | 1540 |
| Sulphur | 0.050 | Tensile strength (MPa) | 750 |
| Phosphorus | 0.050 | Density (kg $m^{-3}$) | 7850 |

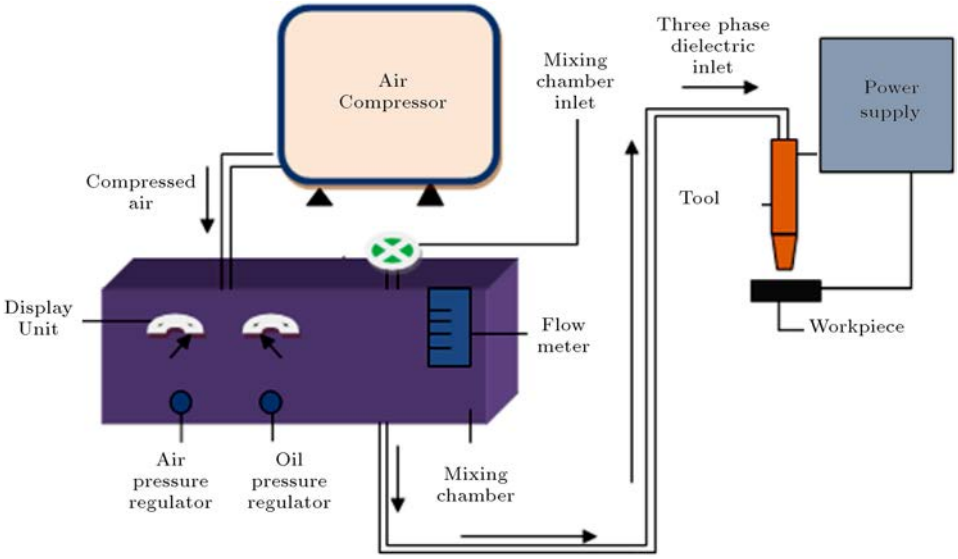


**Figure 10.** Schematic diagram of setup for Powder Mixing Near Dry Electric Discharge Machining (PMND-EDM).

electrodes or the working gap is effective in machining, and it also reduces the need for EDM oil. Unlike the traditional EDM method that requires a large amount of EDM oil, the consumption rate of EDM oil in this method was very small. Therefore, it is necessary to customize a new setup with specifications according to the specified design to meet the research goals and obtain the expected results.

## 5. Results and discussion

### *5.1. Analysis of residual stress*

The workpiece material (EN-31) chosen for residual stress analysis was B.C.C (Body-Centered Cubic) crystal structure with interplanar spacing ($d$) of 1.170 Å, Poisson's ratio of 0.280, diffraction plane ($h$, $k$, $l$) of 2, 1, 1, and with diffraction angle of the X-ray at 156.39 degrees. Figure 11(a)–(i) shows the residual stress analysis of nine series of experiments by X-ray diffractometer according to Taguchi $L_9$ (OA). Figure 11 shows nine sets of experiments based on Taguchi $L_9$ (OA) showing diffraction rings, residual stress, peak profile, and FWHM and their values. Among the experimental values obtained from nine series of experiments, the minimum value of residual stress was found to be 145 MPa. Compared with the high residual stress obtained in the previous work, the obtained residual stress value was much lower [17]. Due to the induced microcracks on the machined surface, the residual stress is reduced. These induced microcracks as shown in Figure 12, were responsible for relieving some of the residual stress, another reason can be attributed to the uniform distribution of heat on the machined surface and improved flushing condition which ultimately relieves some part of the residual stresses on the machined surfaces [22].

The plasma at the machining gap is partially energized by the metal powder concentration, which makes the surface have fewer induced microcracks, as shown in Figure 12. The ionization is improved by adding zinc powder to the dielectric fluid because the added powder expands and widens the discharge gap between the electrodes. This results in the easy removal of debris, which leads to an improvement in surface quality. The results show that by adding the metal powder, the discharge energy dispersion is improved because the dielectric strength of the dielectric fluid decreases with the addition of the metal powder. These favorable conditions improve the forming effect of the machined surface with improved surface characteristics in absence of large cracks [15]. This proves that the metal powder has played an important role in changing the plasma channel. This resulted in improved de-ionization effect and discharging conditions. All these factors increase the discharge frequency as the flushing conditions improve. A mixture of solid and liquid, such as a mist assisted by metal powder, changes the electric field strength of the dielectric medium, thereby facilitating the onset of discharge. Enlarged discharge gap results insufficient heat dissipation, due to which more molten materials will be ejected by the explosive force resulting from the gasification of solid and liquid phases. This phenomenon also restrains the excessive expansion of the discharge channel in its radius. Thus optimal parameters achieve a surface with reduced residual stress.

Table 6 shows the output results of residual stress analysis of nine sets of experiments where $\sigma$ is residual stress, $\sigma_1$ is the standard deviation of residual stress, $\tau_{xy}$ is shear stress, $\sigma_2$ is the standard deviation of shear stress, FWHM is full width half maximum angle, $\alpha_{\max}$

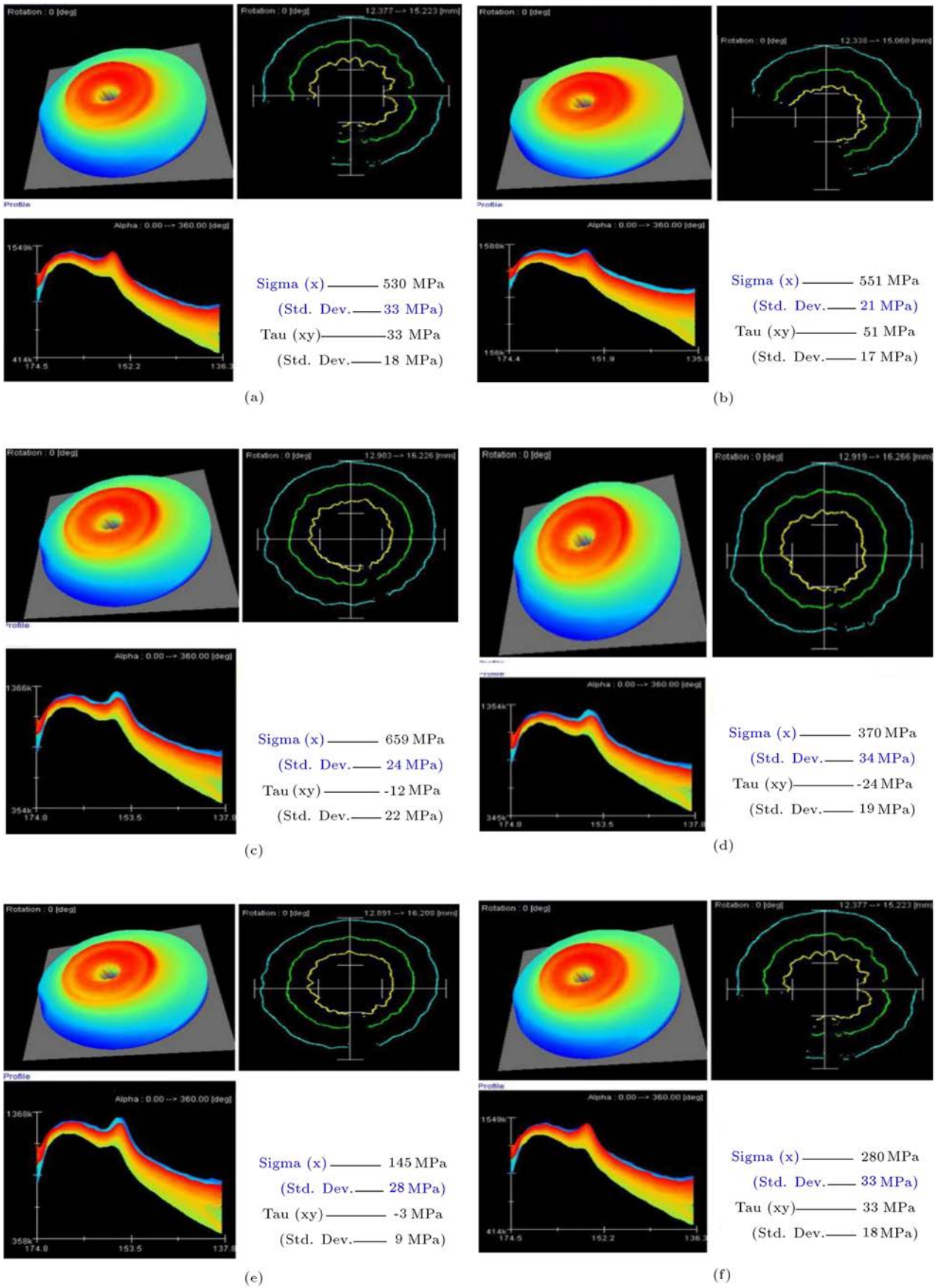


**Figure 11.** Residual stress analysis according to Taguchi $L_9$ (OA).

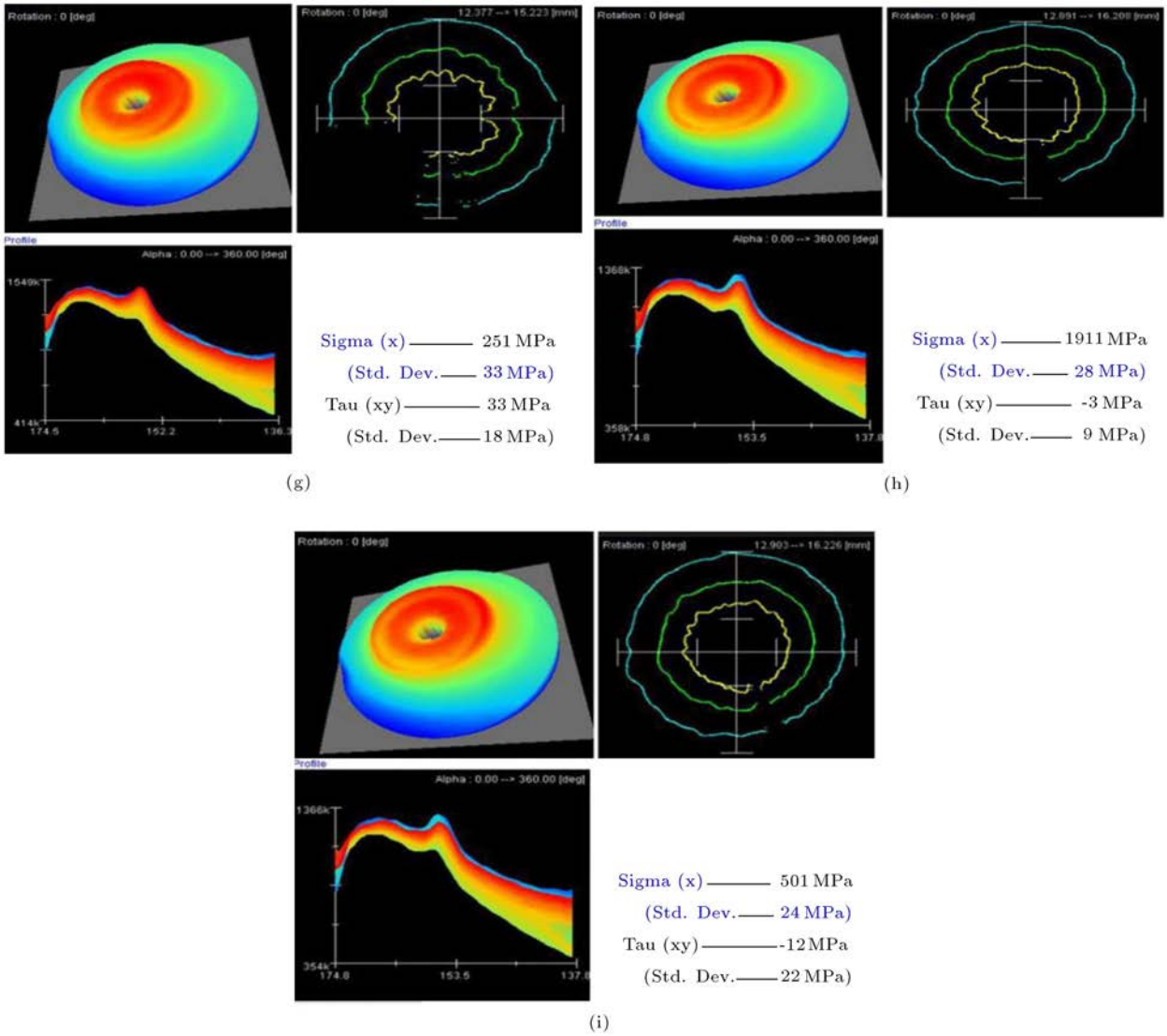


**Figure 11.** Residual stress analysis according to Taguchi $L_9$ (OA) (continued).

**Table 6.** Results obtained by X-ray diffraction testing according to Taguchi $L_9$ (OA).

| Exp. no | RS ($\sigma$) (MPa) | $\sigma_1$ (MPa) | $\tau_{xy}$ (MPa) | $\sigma_2$ (MPa) | FWHM (degree) | $\alpha$-max (degree) | $\alpha$-min (degree) |
|---|---|---|---|---|---|---|---|
| 1 | 530 | 20 | −79 | 11 | 3.49 | 314.60 | 204.48 |
| 2 | 551 | 43 | −61 | 26 | 3.80 | 20.88 | 241.20 |
| 3 | 659 | 49 | 13 | 33 | 3.90 | 83.52 | 200.16 |
| 4 | 370 | 66 | 23 | 53 | 4.42 | 34.56 | 216.72 |
| 5 | 145 | 64 | −199 | 60 | 4.31 | 103.68 | 282.24 |
| 6 | 280 | 19 | −133 | 23 | 3.95 | 39.60 | 216 |
| 7 | 251 | 51 | −63 | 54 | 4.19 | 277.92 | 259.92 |
| 8 | 191 | 81 | −115 | 44 | 4.21 | 161.28 | 110.88 |
| 9 | 280 | 19 | −133 | 23 | 3.95 | 39.60 | 216 |

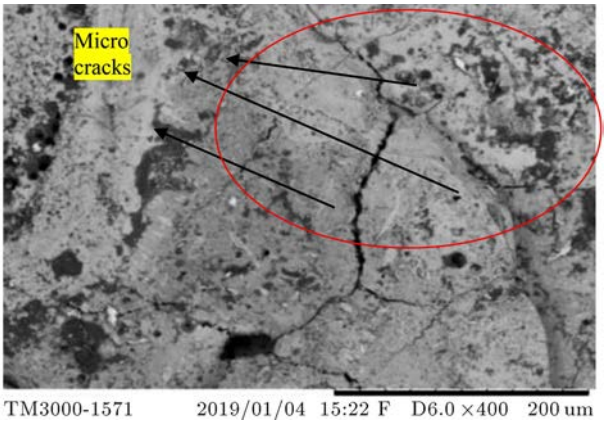


**Figure 12.** Induced micro-cracks in Powder Mixing Near Dry Electric Discharge Machining (PMND-EDM).

is the maximum azimuth angle, and $\alpha_{\min}$ is minimum azimuth angle of debye scherrer ring.

Radial stress analysis on the machined surface was conducted to study the effect of variation of residual stresses with respect to the radial distance from the machined area. The radial residual stress analysis was performed at different radial distances from the center of the machined area.

It was observed that the nature of variation of stress was transforming from tensile to compressive value. Similar trend of residual stress was also observed in previous literature [12–14, 25]. There was a sudden reduction of temperature with respect to an increase in radial distance due to low heat flux in the workpieces. The phenomenon of phase transformation was negligible at a more radial distance from the center of the machined area due to which the grains were again restrained back to compressive nature.

With the help of the residual stress measurement of the machining, shown in Figure 1, the test was performed on different parts of the processed sample. As the radial distance increased further, the thermal effect decreased to a very low value, and finally became negligible at a distance of 1.7 mm, as shown in Figure 13. The average values of residual stresses, main effect values, and S/N ratios of different levels $L_1$, $L_2$, and $L_3$ were calculated, as shown in Tables 7 and 8.

The average values of residual stresses are shown in Figure 14. The parameters $A$, $B$, $C$, and $D$ at levels 2, 2, 1, 2 were most effective in reducing residual stress as shown in Figure14. The same trend for S/N ratios is shown in Figure 14. Parameter $A$ at the 2nd level, parameter B at the 2nd level, parameter $C$ at the 1st level and parameter $D$ at the 2nd level were most effective in reducing residual stress.

The residual stress induced in the workpiece initially decreased with an increase in the inner diameter of the tool-tip at 2nd level ($L_2$). Better flushing occurred on the machined surface which provided a better cooling condition for dissipation of heat on the machined surface. Therefore, less heat was generated on the machined surface which resulted in reducing

**Table 7.** Average values and main effects: Residual Stress, RS (in MPa).

| Process parameter | Level | Tool dia ($A$) | | Flow rate ($B$) | | Powder conc ($C$) | | Pressure ($D$) | |
|---|---|---|---|---|---|---|---|---|---|
| Data type | | S/N | Data raw | S/N | Data raw | S/N | Data raw | S/N | Data raw |
| Average values (% RS) | $L_1$ | −55.29 | 580.22 | −51.41 | 388.88 | −49.93 | 342.33 | −51.36 | 421.88 |
| | $L_2$ | −48.01 | 263.22 | −48.71 | 316.88 | −53.68 | 493.00 | −50.69 | 366.22 |
| | $L_3$ | −49.87 | 338.88 | −53.05 | 476.55 | −49.56 | 347.00 | −51.12 | 394.22 |
| Main effects (% RS) | $L_2$-$L_1$ | 7.27 | −317.00 | 2.69 | −72.00 | −3.74 | 150.66 | 0.67 | −55.66 |
| | $L_3$-$L_2$ | −1.85 | 75.66 | −4.34 | 159.66 | 4.11 | −146.00 | −0.43 | 28 |
| Differences $(L_3$-$L_2)$-$(L_2$-$L_1)$ | | −9.12 | 392.66 | −7.04 | 231.66 | 7.86 | −296.66 | −1.11 | 83.66 |

**Table 8.** ANOVA pooled data for residual stress.

| Source | SS raw | SS S/N | SS' raw | SS' S/N | DOF raw | DOF S/N | Variance raw | Variance S/N | F-ratio raw | F-ratio S/N | $P$% raw | $P$% S/N |
|---|---|---|---|---|---|---|---|---|---|---|---|---|
| Tool diameter | 493368.66 | 85.63 | 489736 | 84.92 | 2 | 2 | 246684.30 | 42.81 | 135.81 | 121.16 | 62.67 | 58.54 |
| Flow rate | 115088.66 | 28.82 | 111456 | 28.11 | 2 | 2 | 57544.33 | 14.41 | 31.68 | 40.78 | 14.61 | 19.70 |
| Powder conc. | 132114.66 | 31.11 | 128482 | 30.40 | 2 | 2 | 66057.33 | 15.55 | 36.36 | 44.02 | 16.78 | 21.27 |
| Mist pressure | 13944.66 | 0.70 | * | - | 2 | – | 6972.33 | * | 3.83 | * | 1.77 | * |
| Error | 32694 | 0.70 | 57536.67 | 2.82 | 18 | 2 | 1816.33 | 0.35 | – | – | 4.15 | 0.48 |
| Total | 787210.66 | 146.27 | 787210.70 | 146.27 | 26 | 8 | * | – | – | – | 100 | 100 |

*Significant at 95% confidence level, F-critical=3.55 (tabular value for raw data), SS: Sum of squares,

DOF: Degree Of Freedom, V: Variance, F-critical=19 (tabular value for S/N data), SS′: Pure sum of squares.

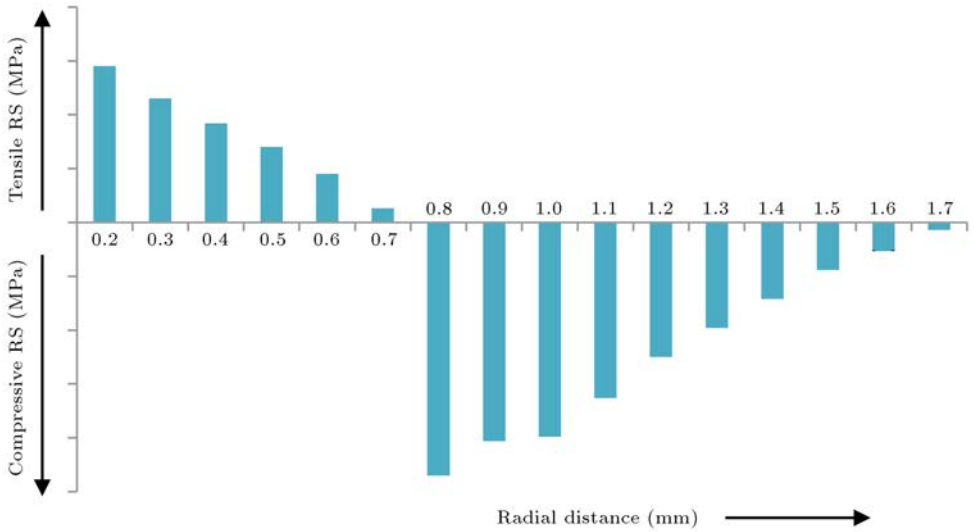


**Figure 13.** Residual stress (MPa) vs radial distance (mm).

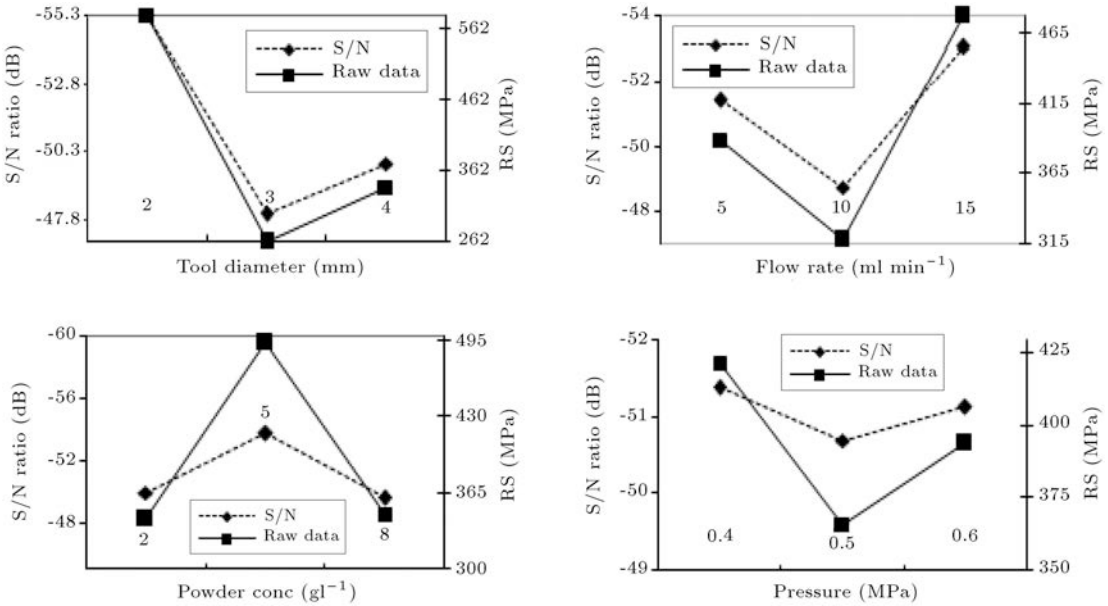


**Figure 14.** Effect of process parameters on Residual Stress (RS) (MPa).

residual stress to the lowest value at $L_2$. At level 3 there was a phenomenon of rapid solidification. This rapid solidification was responsible for an increase in the value of residual stress [25]. Rapid solidification led to the solidification of sputtered melted liquid on the workpiece surface as shown in Figure 15 (scanning electron microscope image). It can be clearly seen from Figure 15 that there is non-homogenous solidified material on the machined surface which was responsible for the change in a specific volume of the molten material and therefore the value of residual stresses was high.

The RS value initially decreased with an increase in flow rate values due to better heat dissipation at $L_2$ but with a further increase of flow rate, there was a phenomenon of stress corrosion due to which the RS value increased to its peak value at $L_3$. Extreme temperature differences are developed on the surface of the machined samples due to high thermal sparking at the inter-electrode gap in EDM. Therefore rapid cooling leads to high residual stresses on the EDM'ed surfaces [15].

The residual stress initially increases with increases in powder concentration but afterward decreases. Due to the low discharge energy density, the spark gap is enlarged, and the addition of metal powder led to the reduction of tensile residual stress. Adding graphite powder to the dielectric will reduce the tensile stress, which in turn also increases the fatigue strength of the machined parts [26]. Due to the presence of metallic powder particles the plasma channel becomes more energized and more heat was is generated on the

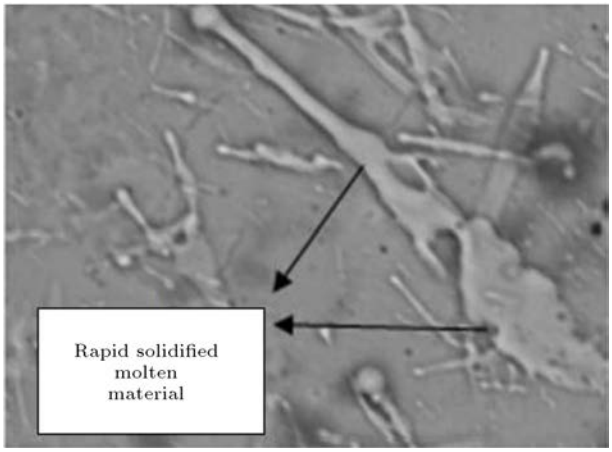


**Figure 15.** Rapid solidification on the surface (SEM image).

workpiece due to which high residual stress was found on the machined surface at $L_2$. As the concentration of metal powder increased, the heat density or heat flux at the machining gap increased exponentially. The bridging effect between the metallic powder particles increases and maintains conditions that are conducive to spark generation, so the temperature of the machined area becomes very high, which is the cause of the higher residual stress value. A further increase in the powder concentration leads to improper spark discharge, thereby reducing the thermal energy of the workpiece. Excessive aggregation of metal powder particles at the inter-electrode gap resulted in the formation of a small thermal plasma, so the thermal intensity at the machining gap is reduced. The lower temperature value at the gap between the electrodes is the cause of the low metallurgical transformation of the machined surface (Scanning Electron Microscope image is shown in Figure 16), which leads to a decrease in the residual stress at $L_3$.

The residual stress value decreased with the increase of the mist pressure and then increased with the further increase of the pressure. The molecular density initially increased as the pressure of the mist increased, thereby improving the deionization effect. These conditions lead to better heat dissipation which reduces residual stress value at $L_2$. The relaxation time for residual stress gets decreased with an increase of mist pressure which led to localized in-homogenous plastic deformation on the machined part as shown in Figure 17 (scanning electron microscope image). These conditions were responsible for the increase in the value of residual stress at $L_3$. Sudden pressure change of mist at $L_3$ was very significant in changing the structure of the grains of the surface layer of the machined part.

*5.1.1. Residual stress performance characteristics estimation*

Response characteristic is determined by the following equation [16]:

$$RS = \bar{A}_2 + \bar{B}_2 + \bar{C}_1 + \bar{D}_2 - 3\overline{RS}. \tag{7}$$

The confidence interval to confirm the experiments is given by Eq. (8) [16]:

$$CI_{CE} = \sqrt{F_\alpha\left(1, f_e\right) V_e \left[\frac{1}{n_{eff}} + \frac{1}{R}\right]}. \tag{8}$$

The Confidence interval of the population is given by Eq. (9) [16]:

$$CI_{POP} = \sqrt{\frac{F_\alpha\left(1, f_e\right) V_e}{n_{eff}}}, \tag{9}$$

where, $F_\alpha(1, fe)$ is the $F$ ratio at the confidence level of $(1-\alpha)$ against DOF 1.

$$F_{0.05}(1, 18) = 3.5546 \text{ (tabulated)}$$

$$n_{eff} = \frac{N}{1 + \text{DOF}} = 9.$$

DOF is associated in the estimation of the mean response. Also, treatment is 9; repetition is 3; $N$(total number of experiments) is 27; $V_e$ (error variance) is 1816.33 (according to Table 8); $f_e$ (error DOF) is 18 (according to Table 9); $R$ (confirmation experiments for sample size) is 3, and:

$$F = \frac{\text{Variation between the samples}}{\text{Variation within the samples}}.$$

**Table 9.** Confirmation experiments for Residual Stress (RS).

| Tool diameter (mm) | Flow rate (ml min$^{-1}$) | Metallic powder concentration (g l$^{-1}$) | Mist pressure (MPa) | Experimental results RS (MPa) | Average RS[a] (MPa) |
|---|---|---|---|---|---|
| 3 | 10 | 2 | 0.5 | 90.32<br>110.39<br>118.49 | 106.40 |

[a]: RS: Residual Stress.

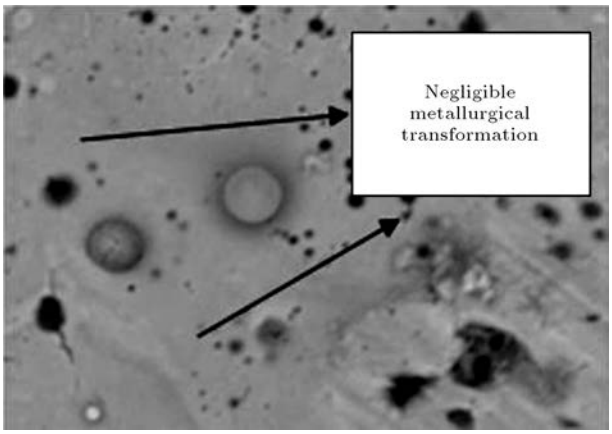


**Figure 16.** SEM image of low metallurgical transformation (SEM image).

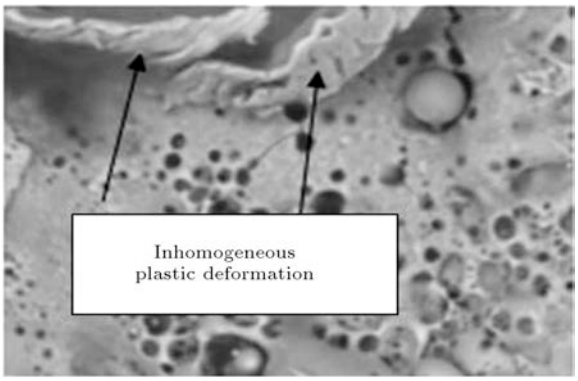


**Figure 17.** Localized in-homogenous plastic deformation (SEM image).

The $F$ value is compared with the $F$ limit for the respective DOF. If the $F$ value is equal to or greater than the $F$ limit value (Table 8), it can be said that significant differences exist between the sample means. So:

$RS = 106.32$ MPa,

$CI_{CE} = \pm 53.56$,

$CI_{POP} = \pm 26.78$.

The predicted optimal range of $CI_{CE}$ is:

Mean $RS - CI_{CE} < RS$(MPa) $<$ mean $RS + CI_{CE}$,

that is, 52.76 MPa $< RS$ (MPa) $<$ 159.88 MPa;

Mean $RS - CI_{POP} < RS$ (MPa) $<$mean $RS + CI_{POP}$,

that is, 79.54 MPa $< RS$ (MPa) $<$133.10 MPa.

*5.1.2. Confirmation experiments for residual stress*
Three repetitions of confirmation experiments for residual stress were performed at optimized levels of process parameters. The residual stress confirmation test was carried out under the experimental conditions of $A_2$, $B_2$, $C_1$, and $D_2$. The experimental residual stresses for three runs under optimized conditions were found to be 90.32 MPa, 110.39 MPa, and 118.49 MPa respectively. The mean experimental residual stress calculated at the optimized process of parameters was 106.40 MPa which was within the confidence interval of predicted residual stress. Thus, the range proved that the predicted value of residual stress lies in the optimum range as shown in Table 9.

## 6. Conclusion

Powder Mixing Near Dry Electric Discharge Machining (PMND-EDM) process is a hybrid method of machining that was efficient in machining rate with improved quality characteristics such as reduced Residual Stress (RS) in the machined product. Optimization technique was utilized in PMND-EDM to study the effect on residual stress. Confirmation experiments were performed at the optimized experimental condition. For the developed settings, the following conclusions can be drawn:

1. When experimenting with optimized process parameter values, it is found that RS had the smallest value. Tool diameter at level 2 (3 mm), the mist flow rate at level 2 (10 ml min$^{-1}$), metallic powder concentration at level 1 (2 g $l^{-1}$), and dielectric mist pressure at level 2 (0.5 MPa) were the most influential values which resulted in lowest RS value of 106.32 MPa in the machined product;
2. The predicted optimal range of residual stress was 52.76 MPa $< RS$ (MPa) $<$ 159.88 MPa. Predicted mean of residual stress at 95% confidence interval was 79.54 MPa $<$ RS (MPa) $<$ 133.10 MPa. This confirms that the average residual stress was within the optimal range of residual stress prediction;
3. Residual stress analysis was performed at a different radial distance from the machined area. It was observed that the residual stresses in the machined area are essentially tensile, but as the radial distance increased, the nature of the residual stress became compressive. The residual stress becomes negligible at a radial distance of 1.7 mm.

### Nomenclature

| | |
|---|---|
| EDM | Electric Discharge Machining |
| DEDM | Dry Electric Discharge Machining |
| NDEDM | Near Dry Electric Discharge Machining |
| PM – EDM | Powder Mixed Electric Discharge Machining |
| PMND – EDM | Powder Mixed Near Dry Electric Discharge Machining |

| | |
|---|---|
| $MRR$ | Material Removal Rate |
| $TWR$ | Tool Wear Rate |
| $Ra$ | Surface finish |
| $RS$ | Residual Stress |
| FWHM | Full Width Half Maximum |
| ANOVA | Analysis of Variance |
| $CI_{ce}$ | Confidence interval of confirmation experiments |
| $CI_{pop}$ | Confidence interval of population |
| $V_e$ | Error variance |
| MH | Micro-Hardness |
| HV | Vickers Hardness number |

## References


1. Kao, C.C., Tao, J., and Shih, A.J. "Near dry electrical discharge machining", *Int. J. Mach. Tool. Manuf.*, **47**, pp. 2273–2281 (2007).
2. Gao, Q., Zhang, Q.H., and Zhang, J.H. "Experimental study of powder-mixed near dry electrical discharge machining", *Chin. J. Mech. Engg.*, **45**, pp. 169–175 (2009).
3. Shen, Y., Liu, H.Y., and Zhang, Y. "High-speed dry electrical discharge machining", *Int. J. Mach. Tool. Manuf.*, **93**, pp. 19–25 (2015).
4. Sundriyal, S., Walia, R.S., and Vipin. "Powder mixed near dry electric discharge machining parameter optimization for tool wear rate", *Advances in Unconventional Machining and Composites. Lecture Notes on Multidisciplinary Industrial Engineering*, Springer, Singapore (2020).
5. Yadav, V.K., Kumar P., and Dvivedi, A. "Performance enhancement of rotary tool near-dry EDM of HSS by supplying oxygen gas in the dielectric medium", *Material. Manuf. Process*, **34**, pp. 1–15 (2019).
6. Yadav, V.K., Kumar, P., and Dvivedi, A. "Effect of tool rotation in near-dry EDM process on machining characteristics of HSS", *Material. Manuf. Process.*, **34**, pp. 779–790 (2019).
7. Sundriyal, S., Walia, R.S., and Vipin. "Near dry and powder mixed near dry electric discharge machining", *Int. J. Engg. Adv. Tech.*, **9**, pp. 2021–2025 (2019).
8. Sundriyal, S., Walia, R.S., Vipin., and Tyagi, M. "Investigation on surface finish in powder mixed near dry electric discharge machining method", *Materials Today: Proceedings*, **25**, pp. 808–809 (2019).
9. Gill, A.S. and Kumar, S. "Investigation of microhardness in electrical discharge alloying of En31 tool steel with Cu-W powder metallurgy electrode", *Arab. J. Sci. Engg.*, **43**, pp. 1499–1510 (2018).
10. Chundru, V.R., Koona, R., and Pujari, S.R. "Surface modification of Ti6Al4V alloy using EDMed electrode made with nano- and micron-sized TiC/Cu powder particles", *Arab. J. Sci. Engg.*, **44**, pp. 1425–1436 (2019).
11. Rahul, Datta, S., and Biswal, B.B. "A novel satisfaction function and distance-based approach for machining performance optimization during electro-discharge machining on super alloy inconel 718", *Arab. J. Sci. Engg.*, **42**, pp. 1999–2020 (2017).
12. Lloyd, H.K. and Warren, R.H. "Metallurgy of spark-machined surfaces", *J. Iron. Steel Inst.*, **203**, pp. 238–247 (1965).
13. Rebelo, J.C., Dias, A.M., and Kremer, D. "Influence of pulse energy on the surface integrity of martensitic steels", *J. Mat. Process. Technol.*, **84**, pp. 90–96 (1998).
14. Crookall, J.R. and Khor, B.C. "Residual stresses and surface effects in electro discharge machining", *Proceedings 13th MTDR Conf.*, Birmingham, pp. 16–27 (1972).
15. Sundriyal, S., Vipin., and Walia, R.S. "Study on the influence of metallic powder in near-dry electric discharge machining", *Strojniški vestnik-J. Mech. Engg.*, **66**, pp. 243–253 (2020).
16. Sundriyal, S., Vipin., and Walia, R.S. "Experimental investigation of the micro-hardness of EN-31 die steel in a powder-mixed near-dry electric discharge machining method", *Strojniški vestnik-J. Mech. Engg.*, **66**, pp. 184–192 (2020).
17. Ekmekci, B., Elkoca, O., and Tekkaya, A.E. "Residual stress state and hardness depth in electric discharge machining: De-ionized water as dielectric liquid", *Mach. Sci. Technology.*, **9**, pp. 39–61 (2007).
18. Ekmekci, B., Tekkaya, A.E., and Erden, A.D. "A semi-empirical approach for residual stresses in electric discharge machining (EDM) ", *Int. J. Mach. Tool. Manuf.*, **46**, pp. 858–868 (2006).
19. Kumar, S., Grover, S., and Walia, R.S. "Effect of hybrid wire EDM conditions on generation of residual stresses in machining of HCHCr D2 tool steel under ultrasonic vibration", *Int. J. Interact. Des. Manuf.*, **12**, pp. 1119–1137 (2018).
20. Liu, J.F. and Guo, Y.B. "Residual stress modeling in Electric Discharge Machining (EDM) by incorporating massive random discharges", *Procedia CIRP.*, **45**, pp. 299–302 (2016).
21. Shabgard, M., Seydi, S., and Seyedzavvar, M. "Novel approach towards finite element analysis of residual stresses in electrical discharge machining process", *Int. J. Adv. Manuf. Technol*, **82**, pp. 1805–1814 (2016).
22. Rao, P.S., Ramji, K., and Satyanarayana, B. "Effect of wire EDM conditions on generation of residual stresses in machining of aluminum 2014 T6 alloy", *Alex. Engg. J.*, **55**, pp. 1077–1084 (2016).
23. Aruja, E. "Displacement of X-Ray Reflexions", *Nature*, **154**(53) (1944).
24. Shen, Y., Liu, Y., and Sun, W. "High-speed near dry electrical discharge machining", *J. Mat. Process. Technol*, **233**, pp. 9–18 (2016).

25. Kruth, J.P. and Bleys, P. "Measuring residual stresses caused by wire EDM of tool steel", *Int. J. Elect. Mach.*, **5**, pp. 23–28 (2000).

26. Talla, G., Gangopadhyay, S., and Biswas, C.K. "Influence of graphite powder mixed EDM on the surface integrity characteristics of inconel 625", *J. Part. Sci. Technol.*, **35**, pp. 219–226 (2016).

## Biographies

**Sanjay Sundriyal** is a PhD student at Delhi Technological University of India. He graduated from the College of Engineering Roorkee and received his masters from the National Institute of Technology Warangal. His research interests are advanced manufacturing processes and optimization.

**Vipin** is a Professor at the Delhi Technological University of India. He received his PhD degree from Delhi Technological University. His area of interest includes advanced manufacturing processes, optimization, and modeling. He has authored many papers, book chapters, conferences, and references papers.

**Ravinderjit Singh Walia** is a Professor at Punjab Engineering College. He received his PhD degree from the Indian Institute of Technology (Roorkee). His area of interest includes advanced manufacturing process, optimization, modeling, and industrial engineering. He is the author of more than 100 papers, book chapters, conferences, and references papers.